CFD-PBM MODELLING OF GAS-LIQUID TWO-PHASE FLOW IN BUBBLE COLUMN REACTORS WITH AN IMPROVED BREAKUP KERNEL ACCOUNTING FOR BUBBLE SHAPE VARIATIONS

Shi W.[a], Li G.[a], Yang J[b], Zong Y.[c], and Yang X.[a]*
*Author for correspondence
E-mail: Xiaogang.Yang @ nottingham.edu.cn
[a] Department of Mechanical, Materials and Manufacturing Engineering,
The University of Nottingham Ningbo China, Ningbo, 315100, PR China
[b] School of Mathematical Sciences,
The University of Nottingham Ningbo China, Ningbo, 315100, PR China,
[c] State Key Laboratory of Chemical Engineering,
East China University of Science and Technology, Shanghai 200237, PR China

ABSTRACT

The breakup model developed by Luo and Svendsen (1993) implemented into CFD modelling of gas-liquid two-phase flows assumes that the bubble shapes are spherical. The simulation results usually yield an unreliable prediction of the break-up of very small bubbles. To the best knowledge of the authors, incorporation of the bubble shape variation into the break-up model has been rarely documented. The current study intends to propose and implement an improved bubble breakup model which accounts for variation of bubble shapes when solving the population balance equations for CFD simulation of gas-liquid two-phase flows in bubble columns.

1. INTRODUCTION

Some previous CFD studies often employ the assumption of an unified bubble diameter, which can only generate accurate predictions if the bubble size distribution is narrow. However, numerical modelling of gas-liquid two-phase flow behaviours has to take into account the bubble size distributions and the bubble-bubble interactions. These are very influential factors in the calculation of the gas-liquid interfacial area, which will further affect the mass and heat transfer between two phases. The multiple size groups (MUSIG) model describes the bubble sizes as being directly derived from the population balance equations (PBE), and the eddy/bubble-bubble interactions being controlled by bubble coalescence and breakup models.

For the bubble breakup process, Coulaloglou and Tavlarides [1] assumed that the breakup process would occur if the energy from turbulent eddies acting on the fluid particle is more than the surface energy it contains. Prince and Blanch [2] acknowledged that bubble breakup was caused by eddy-bubble collision and proposed that the bubble breakup can only be induced by eddies with approximately the same characteristic length. Eddies at a much larger length scale only transport the bubbles without causing breakup. Luo and Svendsen [3] described the bubble breakup by considering both the length scale and the amount of energy contained by the arriving eddies. The minimum length scale of eddies that are responsible for breakup equals to 11.4 times the Kolmogorov scale. The probability for bubble breakup is related to the critical ratio of surface energy increase of bubbles after breakup and the mean turbulent kinetic energy of the colliding eddy. Therefore, very small eddies do not contain sufficient energy to cause the bubble breakup. Lehr, Millies and Mewes [4] proposed a slightly different breakup mechanism from Luo and Svendsen [3]. They considered the minimum length scale of eddies to be determined by the size of the smaller bubble after breakup, and the breakup process to depend on the inertial force of the arriving eddy and the interfacial force of the bubble. Based on the results of Luo and Svendsen [3] and Lehr, Millies and Mewes [4], Wang, Wang and Jin [5] proposed the energy constraint and the capillary constraint criteria for the breakup model. The energy constraint requires the eddy energy to be larger than or equal to the increase of surface energy of bubbles after the breakage. The capillary constraint requires the dynamic pressure of the eddy to exceed the capillary pressure of the bubble. The use of these two breakup criteria actually restricted the minimum size of the bubbles that can break, and hence showed more accurate results than Luo and Svendsen [3]. These two breakup criteria have also been adopted in more recent work by Zhao and Ge [6] and Liao, Rzehak, Lucas and Krepper [7].

2. MATHEMATICAL MODELLING

2.1 Governing equations

A 3D transient CFD model is employed in this work to simulate the local hydrodynamics of the gas-liquid two-phase bubble column. An Eulerian-Eulerian approach is adopted to describe the flow behaviours for both phases, i.e. water as the continuous phase, and air as the dispersed phase.

The mass and momentum balance equations are given by equation (1) and (2) respectively,

$$\frac{\partial(\rho_k \alpha_k)}{\partial t} + \nabla(\rho_k \alpha_k \vec{u}_k) = 0 \tag{1}$$

$$\frac{\partial(\rho_k \alpha_k \vec{u}_k)}{\partial t} + \nabla(\rho_k \alpha_k \vec{u}_k \vec{u}_k) = -\alpha_k \nabla p + \nabla \cdot \overline{\overline{\tau}}_k + \alpha_k \rho_k \vec{g} + \vec{F}_k \tag{2}$$

where ρ_k, α_k, $\vec{u}_k$, $\overline{\overline{\tau}}_k$, and $\vec{F}_k$ represent the density, volume fraction, velocity vector, viscous stress tensor and the inter-phase momentum exchange term for the k (k liquid or gas) phase respectively. The sum of the volume fractions for both phases is equal to 1.

The standard $k \sim \varepsilon$ turbulence model is used for turbulence closure. The turbulent kinetic energy k_l and dissipation rate ε_l are computed by equation (3) and (4),

$$\frac{\partial(\alpha_l \rho_l k_l)}{\partial t} + \nabla \cdot (\alpha_l \rho_l k_l \vec{u}_l) = \nabla \cdot \left[\alpha_l \left(\mu_l + \frac{\mu_{t,l}}{\sigma_k} \right) \nabla k_l \right] + \alpha_l (G_{k,l} - \rho_l \varepsilon_l) \quad (3)$$

$$\frac{\partial(\alpha_l \rho_l \varepsilon_l)}{\partial t} + \nabla \cdot (\alpha_l \rho_l \varepsilon_l \vec{u}_l) = \nabla \cdot \left[\alpha_l \left(\mu_l + \frac{\mu_{t,l}}{\sigma_k} \right) \nabla \varepsilon_l \right] + \alpha_l \frac{\varepsilon_l}{k_l} (C_{1\varepsilon} G_{k,l} - C_{2\varepsilon} \rho_l \varepsilon_l) \quad (4)$$

where $G_{k,l}$ is the production of turbulent kinetic energy and $\mu_{t,l}$ is the turbulent viscosity. In this work, the standard $k \sim \varepsilon$ model constants used are C_μ = 0.09, $C_{1\varepsilon}$ = 1.44, $C_{2\varepsilon}$ = 1.92, σ_k = 1.0, σ_ε = 1.3.

2.2 Bubble size distribution

The bubble size distribution is determined using the MUSIG model, i.e. population balance model with consideration of bubble coalescence and breakup. Bubbles are divided into several size groups with different diameters d_i and an equivalent phase with the Sauter mean diameter to represent the bubble classes. In this study, 16 bubble classes with diameters ranging from 1 to 32 mm are applied based on the geometric discretization method such that $V_i = 2V_{i-1}$. The population balance equation is expressed by equation (5),

$$\frac{\partial n_i}{\partial t} + \nabla \cdot (\vec{v}_i \cdot n_i) = S_i \quad (5)$$

where n_i is the number density for *i*-th group, $\vec{v}_i$ is the mass average velocity vector, and S_i is the source term.

The source term, S_i, for the *i*-th group can be expressed as the birth and death of bubbles due to coalescence and breakup respectively, given by equation (6)

$$S_i = B_{coalescence,i} - D_{coalescence,i} + B_{breakup,i} - D_{breakup,i} = \sum_{d_j = d_{\min}}^{d_i/2} \Omega_C (d_j : d_i - d_j) - \sum_{d_j}^{d_{\max} - d_i} \Omega_C (d_j : d_i) + \sum_{d_j = d_i}^{d_{\max}} \Omega_B (d_j : d_i) - \Omega_B (d_i) \quad (6)$$

The local gas volume fraction can be calculated by equation (7),

$$\alpha_g f_i = n_i V_i \quad (7)$$

where f_i is the *i*-th class fraction of total volume fraction, and V_i is the volume for the *i*-th class.

For the coalescence between two bubbles, the coalescence kernel used in this study was proposed by Luo [8]. As this is not the main concern of this work, further details will not be presented here.

The breakup model used in this work is based on the work of Luo and Svendsen [3]. However, several improvements have been introduced in this study to produce a more realistic breakup model. In Luo and Svendsen's model, the shape of breakage bubbles was assumed to be spherical. However, previous experimental studies, such as Grace, Clift and Weber [9] and Tomiyama [10], have found that the bubbles exist in various shapes and the dynamics of bubble motion strongly depend on the shape of the bubbles. For example, Figure 1 demonstrates the experimentally recorded variation in bubble shapes found in an operating bubble column. The bubble shape has been neglected in previous studies for the simplification of models. However, the shape of the bubbles could potentially be a critical factor for accurately predicting the flow characteristics of the gas phase in CFD simulations.

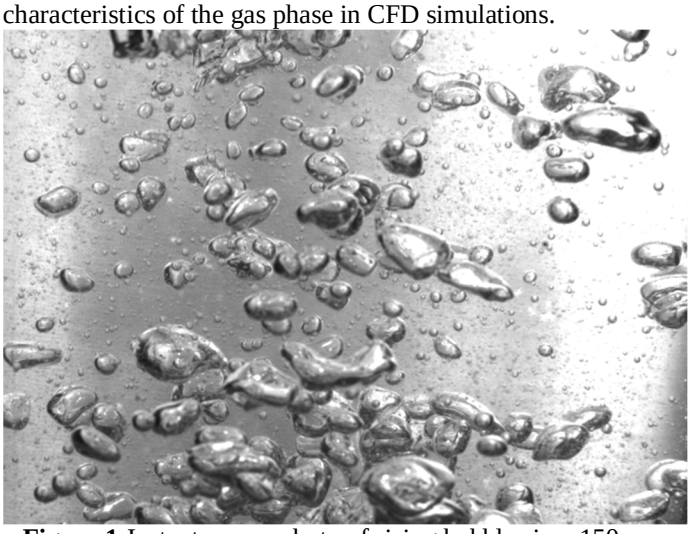

Figure 1 Instantaneous photo of rising bubbles in a 150 mm diameter cylindrical bubble column (*Ug*=0.02 m/s).

From experimental observations, the bubble shapes can be classified into different types. Thus, the effects of different bubble shapes are taken into account in this study. Due to the uncertainty of the spatial rotation of the bubbles, the contact angle of the bombarding eddy is very difficult to be determined. Therefore, instead of the original bubble size, d_i, the equivalent diameter that approximately represents the size of the projected area of the bubble is expressed by equation (8),

$$c \le d_{eq} \le a \quad (8)$$

where *c* and *a* are the length of the short axis and long axis respectively.

The breakup rate for one individual parent bubble breaking into two daughter bubbles is expressed by equation (9),

$$\Omega_B = \int_{\lambda_{\min}}^{d} \omega_B^T p_B d\lambda \quad (9)$$

where ω_B^T is the collision probability density. It can be expressed by using equation (10),

$$\omega_B^T(\xi) = 0.923(1-\alpha_g)(\varepsilon d_i)^{1/3} n_i \frac{(d_{eq,i}/d_i + \xi)^2}{d_i^2 \xi^{11/3}} \quad (10)$$

where $\xi = \lambda / d_i$, characterising the sizes of eddies that may contribute to the breakage of bubble size d_i. The breakage

probability function p_B used by Luo and Svendsen [3] is re-expressed in equation (11),

$$p_B = \exp(-\frac{e_s}{\bar{e}}) \tag{11}$$

where $\bar{e}$ is the mean turbulent kinetic energy for eddies of size λ and e_s is the increase in surface energy of bubbles after breakage. The mean turbulent kinetic energy can be determined by equation (12).

$$\bar{e} = \rho_l \frac{\pi}{6}\lambda^3 \frac{\bar{v}_\lambda^2}{2} = \frac{\pi\beta}{12}\rho_l (\varepsilon d_i)^{2/3} d_i^3 \xi^{11/3} \tag{12}$$

By assuming the bubbles before and after breakage are all in spherical shape, when the parent bubble of size d_i breaks into two bubbles of size d_j and $\left(d_i^3 - d_j^3\right)^{1/3}$, the increase in surface energy was originally described by equation (13),

$$e_s = \sigma \cdot \pi d_i^2 [f_V^{2/3} + (1-f_V)^{2/3} - 1] \tag{13}$$

However, since the effects of different shapes of bubbles are taken into account, equation (13) can be re-written in a general form with regards to the surface area, S, of bubbles, as described by equation (14).

$$e_s = \sigma \cdot (S_{j,1} + S_{j,2} - S_i) \tag{14}$$

According to the models for bubble shapes by Tomiyama, Miyoshi, Tamai, Zun and Sakafuchi [11], there are 3 main types of bubbles that exist in the given conditions in this work, such as the sphere, ellipsoid and spherical-cap. The details of these 3 types of bubbles and their possible breakage footages are given in Figure 2.

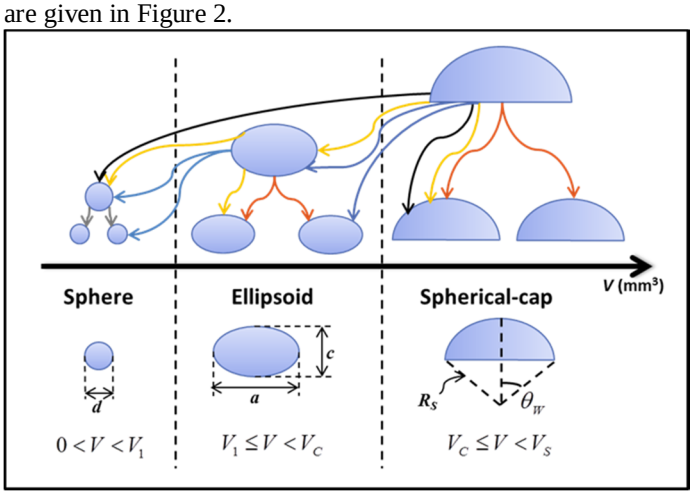

Figure 2 Classification of 3 types of bubbles and the possible breakage footage.

For an air-water system under atmospheric pressure and room temperature, the boundary between spherical bubbles and ellipsoid bubbles, d_1, is 1.16 mm for the pure system and d_1 is 1.36 mm for a slightly contaminated system. The boundary between ellipsoidal and spherical-cap bubbles, d_c, is 17.3 mm under the same conditions. It is very important to point out that the volumes of ellipsoidal bubbles and spherical-cap bubbles are equal to the volumes of their original spherical bubbles with diameter d. For bubbles with ellipsoidal shapes, by assuming an oblate type of ellipsoid, the surface area can be calculated by equation (15),

$$S_{ellipsoid} = \frac{\pi}{2} d^2 E^{1/3} \left(1 + \frac{1}{2E\sqrt{E^2-1}} \ln(2E^2 - 1 + 2E\sqrt{E^2-1})\right) \tag{15}$$

where the aspect ratio E can be expressed using empirical correlation described by Wellek, Agrawal and Skelland [12], as given by equation (16),

$$E = a/b = 1 + 0.163 Eo^{0.757} \tag{16}$$

where Eo is the Eötvös number.

For a single spherical-cap bubble, the wake angle θ_W is also assumed to be 50^o in this work, which is the same as Tomiyama [10]. The curved surface area for the front edge can be calculated using equation (17),

$$S_{Cap} = 2\pi R^2 (1 - \cos\theta_W) \tag{17}$$

where R is the radius of the completed sphere.

It can be seen from the experimental observations by Davenport, Bradshaw and Richardson [13] and Landel, Cossu and Caulfield [14] that the rear surface of a single spherical-cap bubble turns out to be in a constantly oscillating lenticular shape, resulting from the external perturbation acting on the rear surface. However, the lenticular shape rear surface can be considered to be essentially flat, due to the surface energy acting on the curvature which can be averaged over time and hence being neglected. It should be noted that these are rough approximations and more complicated crown bubble systems are not considered in this work. The influence of the variation of bubble shapes on the increase in surface energy is further illustrated in Figure 6.

While the original breakup model only considered the surface energy requirement for breakup events, bubble breakage may also be subjected to the pressure head difference of the bubble and its surrounding eddies, especially when the breakage volume fraction is small. Therefore, on the basis of interaction force balance proposed by Lehr, Millies and Mewes [4], the pressure energy requirement is also considered as a competitive breakup mechanism in this work. The same idea has been adopted by Zhao and Ge [6], Liao, Rzehak, Lucas and Krepper [7], and Guo, Zhou, Li and Chen [15]. The pressure energy requirement can be expressed using equation (18),

$$e_P = \frac{\sigma}{\min(R_{C,j}, R_{C,k})} \cdot \frac{\pi\left(\min\left(d_j, d_k\right)\right)^3}{6} \tag{18}$$

where $R_{C,j}$ and $R_{C,k}$ are the radius of curvature of daughter bubbles. The theoretical prediction of surface energy and pressure energy requirement is shown in Figure 7.

Wang, Wang and Jin [5] proposed the breakage criteria in two aspects: capillary constraint and energy constraint. Due to the consideration of various bubble shapes and the competitive breakup mechanisms, these two constraints cannot be applied to this work directly. Slight modifications are made as follows. When the pressure head of the bombarding eddy is greater than the capillary pressure of the parent bubble, the parent bubble will start to deform. However, as previously mentioned, the breakup event may be subjected to two competitive breakup mechanisms. The energy constraint will be satisfied when the eddy contained energy exceeds either the surface energy or the

pressure energy requirement for forming the daughter bubbles. These two modified breakup criteria will be embedded, together with the previously mentioned surface energy requirement and pressure energy requirement, into the simulation.

The breakup frequency can be obtained by substituting equation (10) ~ (18) into equation (9) and expressed by equation (19),

$$\Omega_B = \begin{cases} 0.923(1-\alpha_g)n_i\left(\frac{\varepsilon}{d_i^2}\right)^{1/3}\int_{\xi_{\min}}^{1}\frac{(d_{eq,i}/d_i+\xi)^2}{\xi^{11/3}}\exp\left(-\frac{12\sigma(S_j+S_k-S_i)}{\pi\beta\rho_L\varepsilon^{2/3}\xi^{11/3}d_i^{11/3}}\right)d\xi, \\ \qquad when\ \frac{6\sigma(S_j+S_k-S_i)}{\pi d_i^2}\geq\frac{\sigma}{\min(R_{C,j},R_{C,k})}. \\ 0.923(1-\alpha_g)n_i\left(\frac{\varepsilon}{d_i^2}\right)^{1/3}\int_{\xi_{\min}}^{1}\frac{(d_{eq,i}/d_i+\xi)^2}{\xi^{11/3}}\exp\left(-\frac{2\sigma(\min(d_j,d_k))^2}{\min(R_{C,j},R_{C,k})\beta\rho_L\varepsilon^{2/3}\xi^{11/3}d_i^{11/3}}\right)d\xi, \\ \qquad when\ \frac{6\sigma(S_j+S_k-S_i)}{\pi d_i^2}<\frac{\sigma}{\min(R_{C,j},R_{C,k})}. \end{cases} \quad (19)$$

where $\xi_{\min}$ is the minimum breakage volume fraction that is able to satisfy both the capillary and the energy constraints.

2.3 Interphase momentum transfer

In this study, drag force, lift force and added mass force are considered as the main interactions between the continuous liquid phase and the dispersed gas phase. The drag force coefficient can be obtained from the model by Grace model [9]. The Grace model is well suited for gas-liquid flows in which the bubbles exhibit a range of shapes, such as sphere, ellipsoid, and spherical-cap. However, instead of comparing the values of drag coefficients in the original Grace model, the drag coefficient can be applied directly according to the actual types of bubbles, as the variation of bubble shapes is considered in the breakup model. Since there are not any further modifications, detailed calculation of the drag force coefficients can be found from Grace, Clift and Weber [9]. The lift coefficient is applied by using the Tomiyama lift force correlation [10]. The virtual mass force coefficient is 0.5 in the present study.

2.4 Numerical modelling

To validate the influence of variations in bubble shape, numerical simulations have been carried out for the air-water bubble column of Kulkarni, Joshi, Kumar and Kulkarni [16], denoted by Case 1, and Camarasa, Vial, Poncin, Wild, Midoux and Bouillard [17], denoted by Case 2. Detailed information is provided in Table 1.

Table 1 Details of experimental set-up.

	Diameter (m)	Height (m)	Superficial Velocity (m/s)	Static liquid Height (m)
Case 1	0.15	0.8	0.0382	0.65
Case 2	0.1	2	0.0606	0.9

As shown in Figure 4, Grid 2 consists of $20(r)\times40(\theta)\times100(z)$ nodes in radial, circumferential and axial directions respectively. The grid independence was tested in a coarser Grid 1 of $16(r)\times32(\theta)\times80(z)$ nodes and a refined Grid 3 of $26(r)\times48(\theta)\times126(z)$ nodes, in which case the total number of cells is doubled gradually. The grid independence test for these three set-ups has yielded similar results quantitatively, even though the overall trend of over-prediction has shown for all three grids, as shown in Figure 5. Thus, Grid 2 shown in Figure 4 is used in the subsequent simulations to investigate the effects of the improved breakup model.

3D pressure-based solver of Fluent® 6.3 is employed for this work. The time step is set to be 0.001 seconds for all simulations. It is considered to be sufficient to illustrate the time-averaged characteristics of the flow fields by carrying out the data sampling statistics for typically 120 seconds after the quasi-steady state is achieved. The improved breakup model is integrated into the simulations by using the user defined function (UDF). The flow chart of the improved breakup model is shown in Figure 3.At inlet boundary, the volume fraction of gas phase is set to be 1 and the velocity profile is applied by using a kinetic inlet model proposed by Shi, Yang and Yang [18]. The outlet boundary is set to be pressure-outlet at the top. No-slip conditions are applied for both liquid and gas phases at the vessel wall.

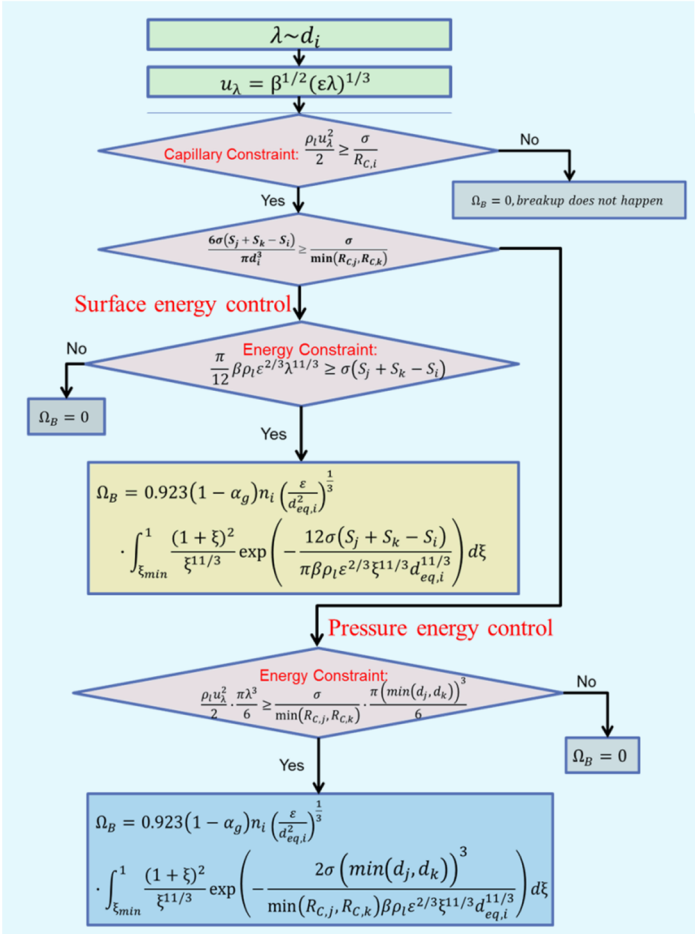

Figure 3 Flow chart of the improved bubble breakup model.

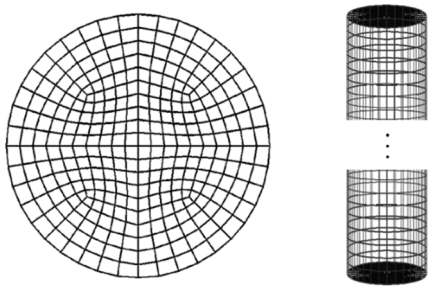

Figure 4 Mesh set-up at the bottom surface and the main body of the column.

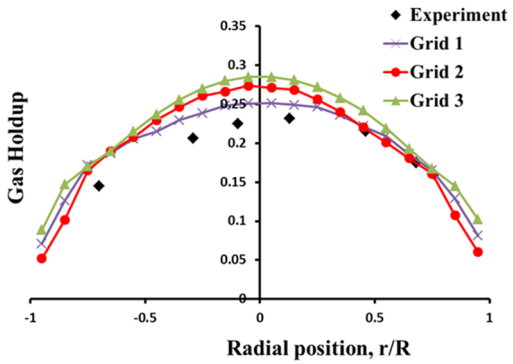

Figure 5 Comparison of simulated gas holdup profile for Case1 with three different grid configurations.

3. RESULTS AND DISCUSSION

To further illustrate the significance of considering the variation of bubble shapes, the theoretical comparison of the increase in surface energy for breakage of original spherical bubbles and various shapes of bubbles is drawn in Figure 6.

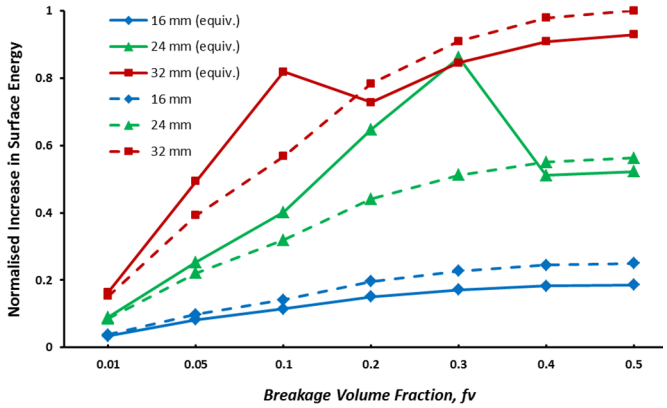

Figure 6 Normalised increase in surface energy for breakage of original spherical bubbles and various shapes of bubbles.

The theoretical predictions of surface energy and the pressure energy requirements for the breakage of ellipsoid and spherical-cap bubble are shown in Figure 7(a) and Figure 7(b) respectively. It can be clearly seen from the Figure 7(a) that the energy requirement for ellipsoid bubble shifts from pressure energy to surface energy with increasing breakup volume fraction. This may be attributed to the situation of the higher pressure head being required inside a smaller bubble to resist the surrounding eddy pressure in order to sustain its own existence. However, as shown in Figure 7(b), the spherical-cap bubble requires mostly surface energy. This may mainly be due to the requirement of forming the large front surface of spherical-cap bubbles.

Figure 8 compares the time averaged gas holdup predicted by the original breakup model and the improved breakup model. It can be seen that the improved breakup model has achieved results very similar to the experimental data at the column centre, while under-estimation is shown near the column wall. Since the standard $k \sim \varepsilon$ turbulence model is still applied in this work, the underestimation of gas holdup may be due to the overestimation of turbulence dissipation rate at this region.

Figure 9 shows the radial distribution of time averaged turbulence dissipation rate predicted by the improved breakup model. It can be seen from equation (19) that the breakup rate Ω_B is at least equivalent to the dissipation rate ε of the order of -1/3, which means the higher dissipation rate near the wall will certainly lead to a lower breakup rate. It is believed that the breakup rate will affect the gas phase volume fraction directly. Moreover, if the Small Perturbation Method can be used to the dissipation term in the equation (4), the dissipation term can be written as:

$$\varepsilon = \varepsilon_0 + \varsigma\varepsilon_1 + \cdots \tag{20}$$

where ς is the small perturbation term that being introduced.

When equation (20) is substituted back into the ε-equation, it can be rewritten in the following cylindrical coordinates if the impacts of axial and circumferential directions can be neglected, as defined in equation (21). The basic approximation can be obtained by finding the zero order of ε term from equation (21), as described by equation (22). The first correction can be obtained by finding the first order of ε term, as denoted by equation (23).

$$\frac{\partial}{\partial r}(\alpha\rho(\varepsilon_0+\varsigma\varepsilon_1)\vec{u}) = \tag{21}$$
$$\frac{\partial}{\partial r}\left[\alpha\left(\mu+\frac{\mu_t}{\sigma_k}\right)\frac{\partial}{\partial r}(\varepsilon_0+\varsigma\varepsilon_1)\right]+\alpha\frac{(\varepsilon_0+\varsigma\varepsilon_1)}{k}(C_{1\varepsilon}G_k - C_{2\varepsilon}\rho(\varepsilon_0+\varsigma\varepsilon_1))$$

$$\mathrm{O}(\varsigma^0):\ C_{01}\frac{\partial}{\partial r}\left(\alpha\frac{\partial\varepsilon_0}{\partial r}\right)+C_{02}\frac{\partial(\alpha\varepsilon_0)}{\partial r}+C_{03}\alpha\varepsilon_0+C_{04}\alpha\varepsilon_0^2=0 \tag{22}$$

$$\mathrm{O}(\varsigma^1):\ C_{11}\frac{\partial}{\partial r}\left(\alpha\frac{\partial\varepsilon_1}{\partial r}\right)+C_{12}\frac{\partial(\alpha\varepsilon_1)}{\partial r}+C_{13}\alpha\varepsilon_1+C_{14}\alpha\varepsilon_0\varepsilon_1=0 \tag{23}$$

It can be seen from the first correction that no matter how small the perturbation on the dissipation term is, the volume fraction term will inevitably generate an opposite feedback effect. This indicates that the overestimation of the dissipation term will indeed lead to the underestimation of gas volume fraction near the wall.

(a)

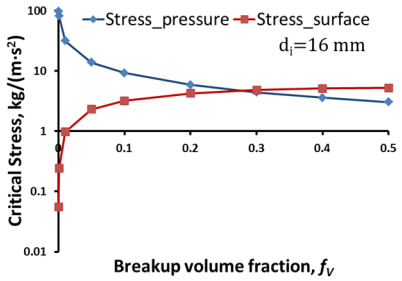

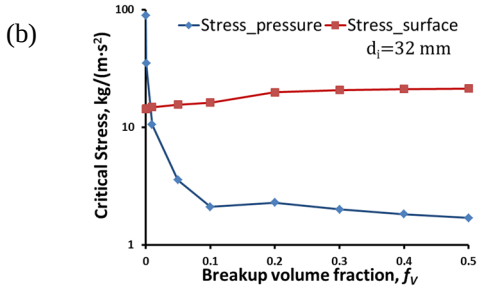

Figure 7 Two competitive control mechanism of the breakage of two types of bubbles: (a) Ellipsoid (b) Spherical-cap.

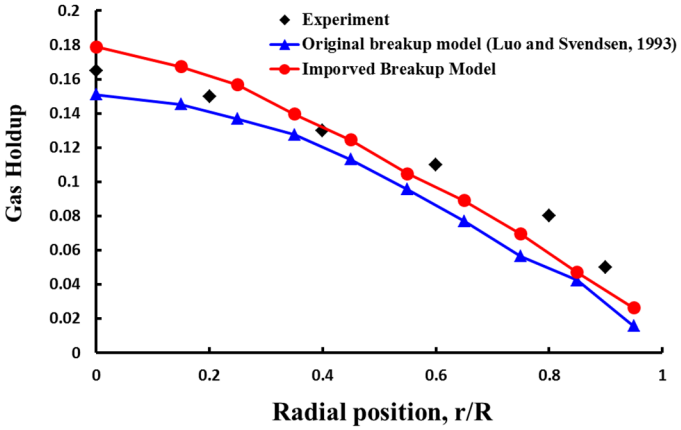

Figure 8 Comparison of the original breakup model and the improved breakup model for Case 1.

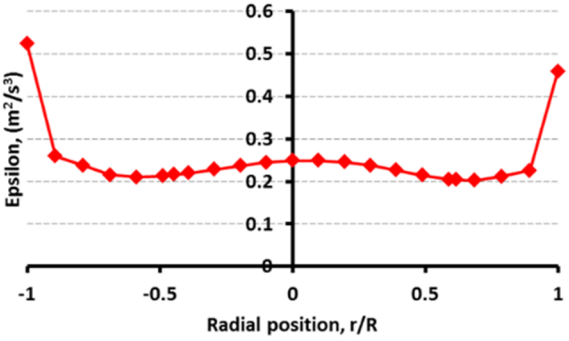

Figure 9 Radial distribution of time averaged turbulence dissipation rate for Case 1.

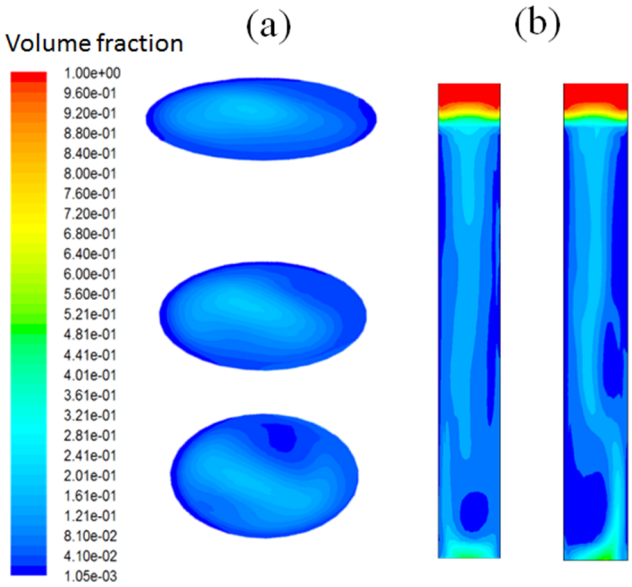

Figure 10 Contours of time averaged gas holdup CASE 1: (a) Aerial view of z-plane: from top to bottom: H=0.6, 0.45, and 0.3 m; (b) x-plane: original breakup model (left) and improved breakup model (right).

Figure 10(a) shows the time averaged gas holdup development obtained by using the improved breakup model. It can be seen from Figure 10(a) that the gas flow is mostly centralised at the column centre even though it moves towards the column wall slightly at the bottom. This is due to the strong vorticity formed at the surrounding region. It can also be observed from Figure 10(b) that the overall flow pattern obtained by the improved breakup model demonstrates significant differences from the original breakup model by Luo and Svendsen [3].

Figure 11 shows the radial distribution of time averaged gas holdup at different cross sections in the axial direction for Case 2. It may be deduced from the Figure 11 that the time averaged flow characteristics in the fully developed region ($H/D>5$) are very similar regardless of the axial positions, and the inlet conditions do not affect this similarity. This result concurs with some previous experimental findings. Figure 12 presents the interfacial area in the bulk region for each bubble group obtained from simulation. Interfacial area is a key parameter that largely affects the prediction of heat and mass transfer between gas and liquid phase in the bubble columns. Although the differences in the simulated interfacial area between the improved breakup model and the original breakup model is not significant when the bubble size is relatively small (bubble volume smaller than 1.309×10^{-5} m^3), the influence of the bubble shapes is gradually reflected when the shape of the bubbles transforms from ellipsoid to spherical-cap, resulting in an increasingly larger interfacial area for large bubbles. The total values of interfacial area in the bulk region are shown in Table 2.

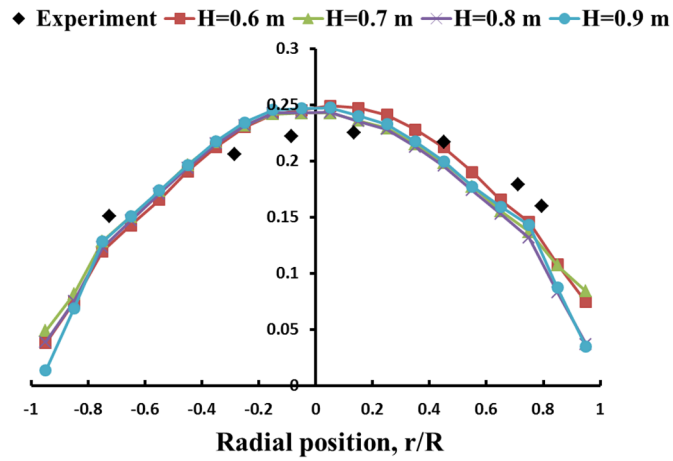

Figure 11 Radial distribution of time averaged gas holdup at different cross sections for Case 2.

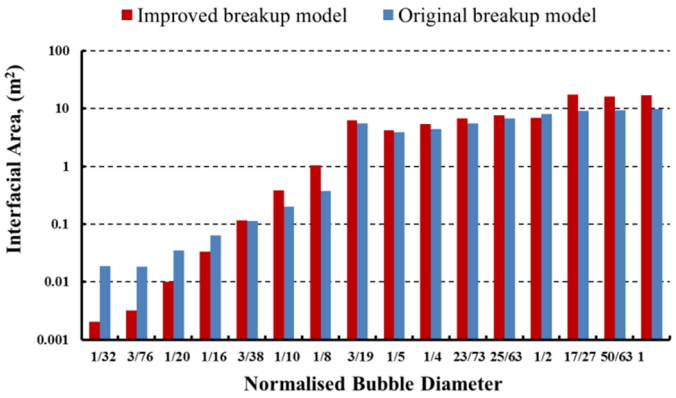

Figure 12 Comparison of simulated interfacial area in the bubble column.

Table 2 Comparison of interfacial area obtained from simulation.

	Improved breakup model	Original breakup model
Interfacial area (m^2)	88.86	62.97

4. CONCLUSIONS

In the present study, an improved breakup model has been proposed based on the classic breakup model of Luo and Svendsen [3]. The improved breakup mode has taken into account the variation of bubble shapes, such as spherical, ellipsoid and spherical-cap in the bubble columns. In addition, the pressure energy controlled breakup coupled with modified breakage criteria has been considered in the present work. The simulation results have achieved very similar findings compared with experimental data. The difference between the surface energy and pressure energy requirements for forming various daughter bubbles has been illustrated. The capillary and energy constraints have been applied to prevent the over-breakage of small bubbles. This study on the dynamic behaviours of various bubble shapes may lead to a more comprehensive understanding of the mass and heat transfer characteristics of the multi-phase reaction in the bubble column.

ACKNOWLEDGEMENTS

The authors gratefully acknowledge the support provided by the National Natural Science Foundation of China (Grant no. 91534118). Weibin Shi would also like to acknowledge the Ph.D. scholarship of the International Doctoral Innovation Centre (IDIC) of University of Nottingham Ningbo China and the support of EPSRC (Grant no. EP/G037345/1).

REFERENCES

[1] C.A. Coulaloglou, L.L. Tavlarides, Description of Interaction Processes in Agitated Liquid-Liquid Dispersions, Chem Eng Sci 32 (1977) 1289-1297.
[2] M.J. Prince, H.W. Blanch, Bubble Coalescence and Break-up in Air-Sparged Bubble-Columns, Aiche J 36 (1990) 1485-1499.
[3] H. Luo, H.F. Svendsen, Theoretical model for drop and bubble breakup in turbulent dispersions, Aiche J 42 (1996) 1225-1233.
[4] F. Lehr, M. Millies, D. Mewes, Bubble-size distributions and flow fields in bubble columns, Aiche J 48 (2002) 2426-2443.
[5] T.F. Wang, J.F. Wang, Y. Jin, A novel theoretical breakup kernel function for bubbles/droplets in a turbulent flow, Chem Eng Sci 58 (2003) 4629-4637.
[6] H. Zhao, W. Ge, A theoretical bubble breakup model for slurry beds or three-phase fluidized beds under high pressure, Chem Eng Sci 62 (2007) 109-115.
[7] Y.X. Liao, R. Rzehak, D. Lucas, E. Krepper, Baseline closure model for dispersed bubbly flow: Bubble coalescence and breakup, Chem Eng Sci 122 (2015) 336-349.
[8] H. Luo, Coalescence, Breakup and Liuqid Circulation in Bubble Column Reactors, PhD thesis from the Norwegian Institute of Technology, Trondheim, Norway, 1993.
[9] J.R. Grace, R. Clift, M.E. Weber, Bubbles, Drops, and Particles, Academic Press1978.
[10] A. Tomiyama, Struggle with computational bubble dynamics, Multiphase Science and Technology, Vol 10 Issue 4 1998 (1998) 369-405.
[11] A. Tomiyama, K. Miyoshi, H. Tamai, I. Zun, T. Sakafuchi, A Bubble Tracking Method for the Prediction of Spatial-Evolution of Bubble Flow in a Vertical Pipe, 3rd International Conference on Multiphase Flow (ICMF 98)Lyon, France, 1998.
[12] R.M. Wellek, A.K. Agrawal, A.H. Skelland, Shape of Liquid Drops Moving in Liquid Media, Aiche J 12 (1966) 854-&.
[13] W.G. Davenport, A.V. Bradshaw, F.D. Richardson, Behaviour of Spherical Cap Bubbles in Liquid Metals, J Iron Steel I 205 (1967) 1034-1042.
[14] J.R. Landel, C. Cossu, C.P. Caulfield, Spherical cap bubbles with a toroidal bubbly wake, Phys Fluids 20 (2008).
[15] X.F. Guo, Q. Zhou, J. Li, C.X. Chen, Implementation of an improved bubble breakup model for TFM-PBM simulations of gas-liquid flows in bubble columns, Chem Eng Sci 152 (2016) 255-266.
[16] A.A. Kulkarni, J.B. Joshi, V.R. Kumar, B.D. Kulkarni, Application of multiresolution analysis for simultaneous measurement of gas and liquid velocities and fractional gas hold-up in bubble column using LDA, Chem Eng Sci 56 (2001) 5037-5048.
[17] E. Camarasa, C. Vial, S. Poncin, G. Wild, N. Midoux, J. Bouillard, Influence of coalescence behaviour of the liquid and of gas sparging on hydrodynamics and bubble characteristics in a bubble column, Chem Eng Process 38 (1999) 329-344.
[18] W. Shi, N. Yang, X. Yang, A kinetic inlet model for CFD simulation of large-scale bubble columns, Chem Eng Sci 158 (2017) 108-116.